Hindawi Publishing Corporation
Journal of Nanomaterials
Volume 2011, Article ID 469685, 6 pages
doi:10.1155/2011/469685

Research Article

Particle Size Control of Y_2O_3:Eu^{3+} Prepared via a Coconut Water-Assisted Sol-Gel Method

Maria de Andrade Gomes, Mário Ernesto Giroldo Valerio, and Zélia Soares Macedo

Laboratory of Advanced Ceramic Materials, Physics Department, Federal University of Sergipe, 49100-000 São Cristóvão, SE, Brazil

Correspondence should be addressed to Zélia Soares Macedo, zelia.macedo@gmail.com

Received 2 October 2010; Revised 24 November 2010; Accepted 23 December 2010

Academic Editor: Yanan Du

Eu^{3+}-doped Y_2O_3 nanoparticles were produced through proteic sol-gel technique, and the adjustment of pH was tested in order to control the particle size of the powders. A strong correlation between the initial pH and the temperature of crystallization was observed, allowing the production of particles with controlled diameter from 4 nm to 50 nm. The samples were characterized by X-ray diffraction, high-resolution transmission electron microscopy, optical microscopy and photoluminescence spectroscopy in both absorption and emission modes. A blue shift of the excitation peak corresponding to energy transfer from Y_2O_3:Eu^{3+} host to Eu^{3+} ions was observed, as the particle size was reduced from 50 to 4 nm. The suppression of a charge transfer band also resulted from the reduction of the particle size. The emission spectrum of the Y_2O_3: with particles of 50 nm was found to be similar to that of bulk material whereas 4 nm particles presented broadened emission peaks with lower intensities.

1. Introduction

There is currently a great deal of interest on the development of luminescent nanoparticles for biomedical applications. Compared to traditional organic dyes and fluorescent proteins, inorganic phosphors can offer several advantages such as tunable emission from visible to infrared wavelengths, large absorption coefficient across a wide spectral range, high quantum yield and stability against photobleaching [1]. In the past few years, luminescent quantum dots (QDs) have been investigated aiming their application as labels in biosensing and imaging [2–6]. However, one of the major concerns in the medical applications of QDs is their inherent toxicity, since the most widely used QDs probes, like CdSe, CdTe, CdS, PbSe and ZnSe, are heavy metal-based materials. A number of mechanisms, such as free radical formation of heavy metal, interaction of QDs with intracellular components and surface oxidation, have been postulated to be responsible for QDs cytotoxicity [5, 6]. Considering these limitations, the production of heavy metal-free luminescent nanoparticles becomes a matter of the highest importance and rare earth-doped nanocrystals are pointed out as the best candidates to substitute QDs luminescent probes [7–10].

Amongst a variety of luminescent rare earth-doped systems, Eu^{3+}-doped Y_2O_3 shows the highest quantum efficiency (almost 100%), and it is widely investigated for applications in fluorescent lamps, display panels and luminescent inks [11–13]. Different methods have been employed to produce nanocrystalline Y_2O_3:Eu^{3+} [14–16]. In this work, a coconut water-based sol-gel synthesis, also known as proteic sol-gel route, was investigated. The advantages of this new method are the simplicity and low environmental impact, since it employs the protein chains of coconut water and metal salts in substitution of alcoxide precursors [17].

As it is widely known, the reactivity of the particles increases as their size decreases. This high reactivity leads to the agglomeration of these small particles and can result in undesirable coalescence [18] during thermal treatments for the crystallization of the samples. On the other hand, there are reports on the influence of pH on the agglomeration degree and particle size of the materials produced by wet chemistry and combustion synthesis [19–21]. In a previous work, the proteic sol-gel route was used, without

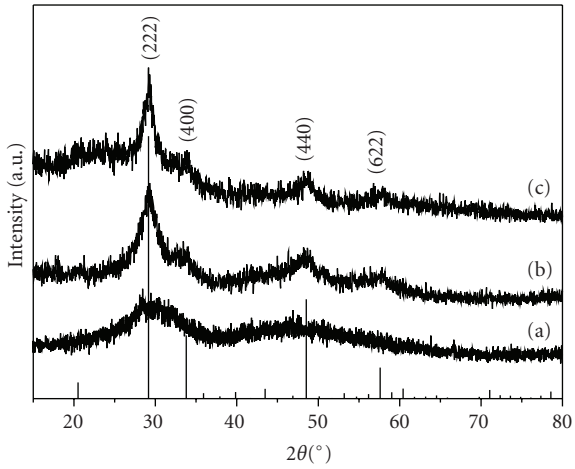

FIGURE 1: X-ray diffraction patterns of Y_2O_3:Eu^{3+} produced by sol-gel with pH control: (a) amorphous phase (xerogel), (b) pH = 7.0, crystallised at 350°C and (c) pH = 9.0, crystallised at 400°C.

pH control, to produce Y_2O_3 [22]. The smallest particles obtained by this method sized 50 nm. In the present work, the adjustment of the pH during the synthesis was tested in order to produce even smaller particles, establishing a direct relationship between the initial pH and the final granulometry of the powders. The influence of the particle size on the luminescent properties of these phosphors are also presented and discussed.

2. Experimental

The Y_2O_3:Eu^{3+} nanopowders were prepared via proteic sol-gel [17] using the salts $Y(NO_3)_3$ and $Eu(NO_3)_3$ (Alfa Aesar, grade purity 99.99%) as precursor materials. These reactants were mixed with processed coconut water, according to the formula $(Y_{0.98}Eu_{0.02})_2O_3$, and homogenized by stirring at room temperature. In this route, the metal ions are believed to bind to the polymeric chains present in coconut water, forming a colloidal suspension (sol). To adjust pH, ammonium hydroxide, NH_4OH (Vetec, P.A.) was added drop by drop into the sol, while it was stirred, and the pH values of the sol were monitored using a Lutron 206 pH meter. It has been reported that the pH of the solution can modify the size of nanoparticles [19–21]. The pH values investigated in this work were 5.0, 7.0, and 9.0. A sample without pH control was also produced and used as reference. After stirring for 10 minutes, the sol was polymerized and formed a gel, which was dried at 100°C/24 hours. The dried material (aerogel) was homogenized and calcined to reach the crystalline phase. Several calcination temperatures were tested from 300°C up to 850°C. After the calcinations, the samples were washed in distilled water to eliminate residual KCl phase, which is an ionic salt present in coconut water.

The crystalline phase of the powders was inspected by X-ray diffraction (XRD-Rigaku RINT 2000/PC) in continuous scanning mode using Cu K_α radiation. The average crystallite size of the samples was obtained from the full width at half maximum (FWHM) of the diffraction peaks, with instrumental correction using LaB_6 standard powder [20, 23]. Transmission electron microscopy (TEM) images were obtained with a Tecnai 20 microscope and they were used to analyse morphology and size of the produced nanoparticles. Micrographs of the samples illuminated with ultraviolet (UV) light were obtained with an optical microscope. For both electron and optical microscopy, the powders were dispersed in isopropyl alcohol with the aid of an ultrasonic bath.

The optical properties of the Eu^{3+}-doped Y_2O_3 samples were inspected via photoluminescence technique in emission and excitation modes. These optical spectra were acquired at room temperature in an ISS PC1TM spectrofluorometer that uses a 300 W Xenon lamp as excitation source. The emission spectra were measured with excitation fixed at 245 nm whereas the excitation spectra were measured by monitoring the intensity of luminescence at 614 nm ($^5D_0 \rightarrow {}^7F_2$ transition of Eu^{3+}).

3. Results and Discussion

Figure 1 presents the X-ray diffraction patterns of 2% Eu^{3+}-doped Y_2O_3 nanocrystals produced at pH = 7.0 and pH = 9.0. For all the samples studied, the obtained XRD patterns were consistent with the cubic phase of Y_2O_3 with spatial group Ia3 (JCPDS No 79-1257). The most intense peaks correspond to the crystal planes (222), (400), (440), and (622). These peaks are broadened due to the small size of the nanoparticles. From the diffraction patterns, one can observe that the sample produced at pH = 7.0 was crystallised after calcination at 350°C. At this temperature, all the other samples were amorphous. For the sample synthesized at pH = 9.0, the lowest crystallization temperature was 400°C and the other samples only presented crystalline structure after calcinations at 450°C.

The crystallite size could be estimated from the FWHM of the diffraction peaks using Scherrer's equation $d = K\lambda/(\beta \cdot \cos\theta_B)$, where K is the shape coefficient for the reciprocal lattice point (in this work $K = 0.89$), λ is the wavelength of the X-rays ($\lambda = 0.15405$ nm), θ_B is the peak position, and $\beta = \sqrt{B^2 - b^2}$ is the width of specimen's peak (B) corrected by a instrumental broad factor (in this work, $b = 0.005192$ rad). The results are presented in Table 1, where it can be observed that the biggest crystallite size were obtained for the sample calcined at 850°C, departing from the sol without pH control. The smallest crystallites were produced at pH = 7.0 and T = 350°C. As expected, the samples calcined at lower temperatures presented smaller crystallites. One can also observe that the particles produced at pH = 7.0 present a pronounced growth at 500°C, reaching the average size of 18 nm whereas the samples produced at lower pH values remain smaller than 10 nm at this temperature.

The reduction of the surface energy is the driving force for both nucleation and particle growth. This thermodynamic parameter depends on the surface tension of curved interfaces and also on the net surface area of the particles [24]. Nanoparticles have high surface energy due

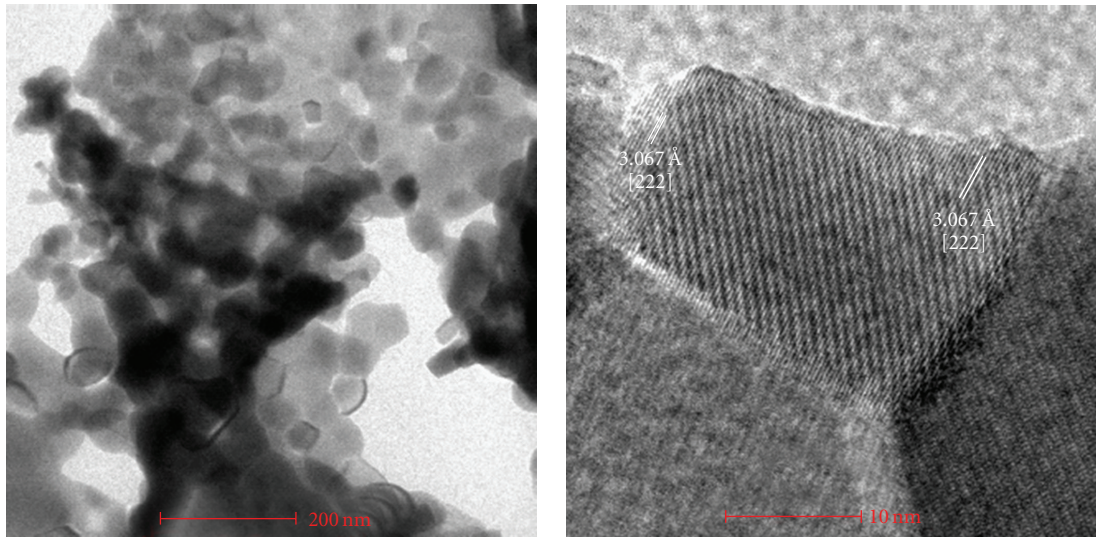

(a) (b)

Figure 2: Micrographs of powder produced at pH = 7.0 and calcined at 500°C. (a) TEM image showing spherical-like produced particles. (b) HRTEM image indicating that each particle contains only one crystallite.

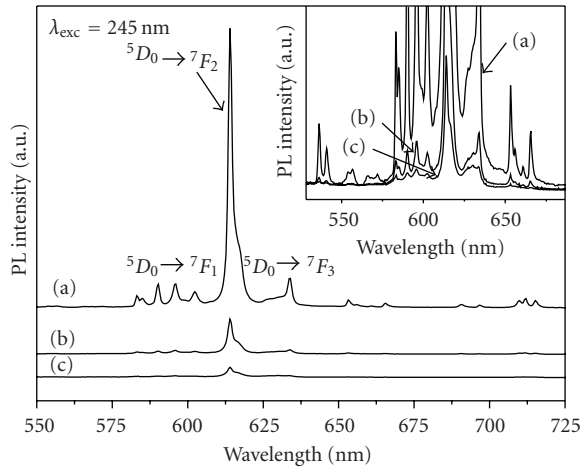

Figure 3: Emission spectra of Y_2O_3:Eu^{3+} nanocrystals with particle sizes of 50 nm (curve a), 7 nm (curve b), and 4 nm (curve c).

to the small curvature radius and large surface area, so the system spontaneously tends to decrease the interface solid solution, and particles tend to grow in order to minimize the surface energy. On the other hand, the surface tension (and, consequently, the surface energy) of particles in suspension can be decreased by adsorption of the amine groups from the ammonium hydroxide [25], which promote both electrostatic and steric stabilization of nanoparticles. This stabilization prevents the grown of the particles, so the acidity of the medium of synthesis strongly influences the particle size [26]. Besides that, as temperature can also influence surface energy [26], lowering the synthesis

Table 1: Crystallite size of the Y_2O_3:Eu^{3+}-particles produced by proteic sol-gel as a function of pH and temperature (n.d. stands for not determined).

	Without pH control	pH = 5.0	pH = 7.0	pH = 9.0
T = 350°C	amorphous	amorphous	3 nm	amorphous
T = 400°C	amorphous	amorphous	4 nm	6 nm
T = 450°C	7 nm	7 nm	5 nm	7 nm
T = 500°C	9 nm	9 nm	18 nm	n.d.
T = 850°C	50 nm	n.d.	n.d.	n.d.

temperature results in a wider size distribution with an increased amount of small particles.

Figure 2 presents TEM images of the powder prepared at pH = 7.0 and treated at 500°C. In Figure 2(a), one can observe spherical-like particles with reduced agglomeration degree when compared with the results from other synthesis methods [11]. For the samples shown in Figure 2, the average particle size observed in the micrographs was 20 nm, which agrees with the crystallite size determined from the X-ray diffraction patterns (see Table 1). Figure 2(b) presents the high-resolution (HRTEM) image of the same sample, where one can observe the lattice planes indicating that each particle contains only one crystallite. Consequently, the crystallite sizes presented in Table 1 can be interpreted as the average particle size of the samples. In Figure 2(b), the distance between [222] family planes is 3.067 Å, which is consistent with the value of 3.066 Å obtained from crystallographic database [27].

One important step on the development of alternative nontoxic nanocrystals for biomedical imaging is the

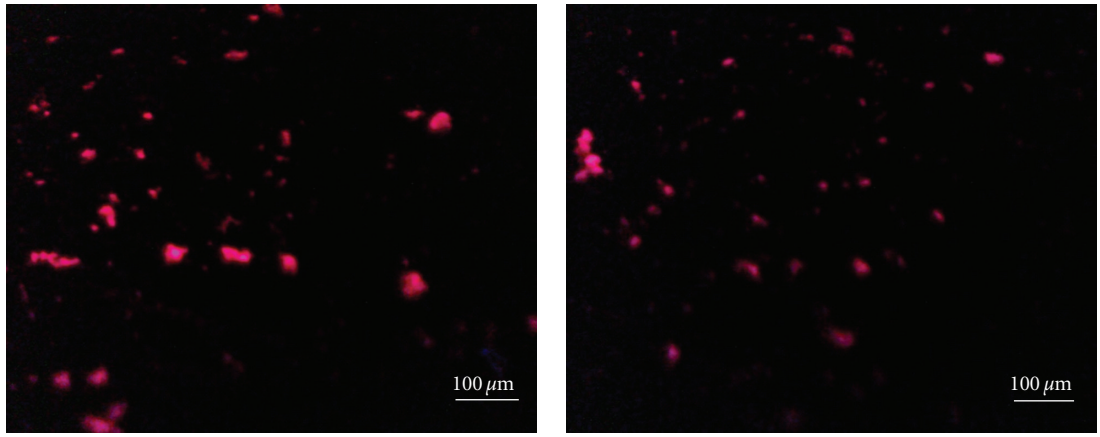

(a) (b)

FIGURE 4: Micrographs of Y_2O_3:Eu^{3+} produced by proteic sol-gel: (a) without pH control and calcined at 850°C and (b) at pH = 7.0 and calcined at 350°C. The images were registered during illumination with UV light.

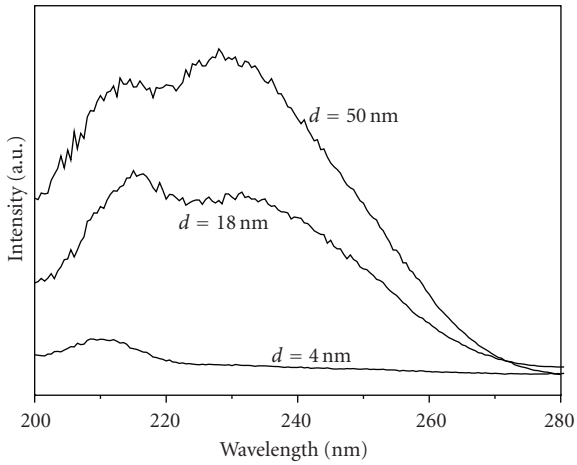

FIGURE 5: Excitation spectra of Y_2O_3:Eu^{3+} nanocrystals with average particle size of 4, 18, and 50 nm, monitored for $^5D_0 \rightarrow {}^7F_2$ (614 nm) emission.

investigation of their luminescence properties. In this work, the emission and excitation spectra of doped Y_2O_3:Eu^{3+} produced by proteic sol-gel were measured for samples with different particle sizes. Figure 3 presents the emission spectra for samples with particle sizes of 50 nm (curve a), 7 nm (curve b), and 4 nm (curve c), under excitation of 245 nm. In these spectra, the intensity was normalized by the excitation intensity (I_0), so the luminescent intensities are comparable. For particle sizes of 50 nm, the features of the emission spectrum are similar to those of the bulk material [28]. The main peak at 614 nm originates from $^5D_0 \rightarrow {}^7F_2$ forced electric-dipole transition of Eu^{3+}; the one centered at 633 nm corresponds to $^5D_0 \rightarrow {}^7F_3$ transition and the peaks around 595 nm correspond to $^5D_0 \rightarrow {}^7F_1$ transition, which is a magnetic-dipole transition [29]. For the samples with average diameter of 7 and 4 nm, the emission peaks are at the same positions, indicating the same electronic transitions, but they are significantly broadened due to local disorder surrounding the Eu^{3+} ions. The intensity of luminescence also depends on the particle size and this dependence should be taken into account for the application of these nanoparticles as biological labels. At 614 nm, the intensity of the 4 nm particles is 3.3% of that observed for the 50 nm particles. On the other hand, the dimensional similarity of the smaller particles with some biological macromolecules such as nucleic acids and proteins would allow a better integration of these nanoparticles with biological systems, with possible applications in medical diagnostics and targeted therapeutics. Figure 4 presents the images obtained with optical microscope (magnification of 400x) of the powder samples with particle diameter of 50 nm (Figure 4(a)) and 4 nm particles (Figure 4(b)), under UV excitation. Due to the low magnification, it is not possible to distinguish isolated particles, but from these images, it can be concluded that the luminescence of the smaller particles is still strong enough to be detected by fluorescence microscopy techniques.

The excitation spectra for the $^5D_0 \rightarrow {}^7F_2$ transition of Eu^{3+} is presented in Figure 5 for the samples with particle sizes of 50 nm, 18 nm and 4 nm. For smaller particles, it is observed a lower overall intensity of the spectra, compared to the 50 nm sample. An excitation band near 214 nm was observed for all the samples and was assigned to the energy transfer excitation from the Y_2O_3 host to Eu^{3+} [30]. This band is slightly blue shifted to 209 nm for the 4 nm sample. For the particles with average size of 50 nm and 18 nm, it is also observed a band at around 210 nm, which is associated with a charge transfer (CT) from O^{2-} to Eu^{3+}. Electrons from the 2p orbital of oxygen are transferred to the $^5D_0$ excited level of Eu^{3+}, and the red light is emitted when the decay $^5D_0 \rightarrow {}^7F_2$ occurs [31]. As the CT band is especially sensitive to the local order surrounding O^{2-}, its intensity is reduced for the particles with 18 nm and suppressed for the particles with 4 nm. Similar behaviour was ascribed by other authors to Y_2O_3:Eu^{3+} particles smaller than 10 nm [30].

4. Conclusions

Size-controlled Y_2O_3:Eu^{3+} nanoparticles were successfully obtained via proteic sol-gel with pH adjustment at the initial stage of the synthesis. The average particle size was tunable from 4 to 50 nm by the control of the pH and calcination temperature of the samples. The advantages of this synthesis route are the simplicity, low environmental impact, and low cost of production, since it employs a natural resource (coconut water) instead of the conventional metallic alkoxides. The temperature of 350°C, used for the production of particles with average diameter of 4 nm, is at least 500°C lower than those reported in the literature for the crystallization of this material [22]. The luminescent characterization of the samples has shown a dependence of the quantum yield on the particle size, probably related to the suppression of the charge transfer from the oxygen to the excited level of Eu^{3+}. Nevertheless, the particles with diameter of 4 nm still presented strong red emission, suggesting that they are suitable to be used in conjugation with biological systems. These conjugation tests are currently being performed in our research group.

Acknowledgments

The authors wish to acknowledge CETENE for the use of microscopy facilities and the financial agencies CNPq, CAPES, FINEP, and FAPITEC/SE.

References

[1] X. Gao, L. Yang, J. A. Petros, F. F. Marshall, J. W. Simons, and S. Nie, "*In vivo* molecular and cellular imaging with quantum dots," *Current Opinion in Biotechnology*, vol. 16, no. 1, pp. 63–72, 2005.

[2] R. Dey, S. Mazumder, M. K. Mitra, S. Mukherjee, and G. C. Das, "Review: biofunctionalized quantum dots in biology and medicine," *Journal of Nanomaterials*, vol. 2009, Article ID 815734, 17 pages, 2009.

[3] W. Zhong, "Nanomaterials in fluorescence-based biosensing," *Analytical and Bioanalytical Chemistry*, vol. 394, no. 1, pp. 47–59, 2009.

[4] A. M. Smith, G. Ruan, M. N. Rhyner, and S. Nie, "Engineering luminescent quantum dots for in vivo molecular and cellular imaging," *Annals of Biomedical Engineering*, vol. 34, no. 1, pp. 3–14, 2006.

[5] A. P. Alivisatos, W. Gu, and C. Larabell, "Quantum dots as cellular probes," *Annual Review of Biomedical Engineering*, vol. 7, pp. 55–76, 2005.

[6] T. Jamieson, R. Bakhshi, D. Petrova, R. Pocock, M. Imani, and A. M. Seifalian, "Biological applications of quantum dots," *Biomaterials*, vol. 28, no. 31, pp. 4717–4732, 2007.

[7] W. Cai, A. R. Hsu, Z. B. Li, and X. Chen, "Are quantum dots ready for in vivo imaging in human subjects?" *Nanoscale Research Letters*, vol. 2, no. 6, pp. 265–281, 2007.

[8] J. Yuan and G. Wang, "Lanthanide-based luminescence probes and time-resolved luminescence bioassays," *Trends in Analytical Chemistry*, vol. 25, no. 5, pp. 490–500, 2006.

[9] N. Pradhan, D. M. Battaglia, Y. Liu, and X. Peng, "Efficient, stable, small, and water-soluble doped ZnSe nanocrystal emitters as non-cadmium biomedical labels," *Nano Letters*, vol. 7, no. 2, pp. 312–317, 2007.

[10] K. Manzoor, S. Johny, D. Thomas, S. Setua, D. Menon, and S. Nair, "Bio-conjugated luminescent quantum dots of doped ZnS: a cyto-friendly system for targeted cancer imaging," *Nanotechnology*, vol. 20, no. 6, p. 113, 2009.

[11] Z. Wei-Wei, X. Mei, Z. Wei-Ping et al., "Site-selective spectra and time-resolved spectra of nanocrystalline Y_2O_3:Eu," *Chemical Physics Letters*, vol. 376, no. 3-4, pp. 318–323, 2003.

[12] M. Abdullah, . Astuti, and . Khairurrijal, "Synthesis of luminescent ink from europium-doped Y_2O_3 dispersed in polyvinyl alcohol solution," *Advances in OptoElectronics*, vol. 2009, Article ID 918351, 8 pages, 2009.

[13] P. Psuja, D. Hreniak, and W. Strek, "Rare-earth doped nanocrystalline phosphors for field emission displays," *Journal of Nanomaterials*, vol. 2007, Article ID 81350, 7 pages, 2007.

[14] B. Bihari, H. Eilers, and B. M. Tissue, "Spectra and dynamics of monoclinic Y_2O_3 and Eu^{3+}: Y_2O_3 nanocrystals," *Journal of Luminescence*, vol. 75, no. 1, pp. 1–10, 1997.

[15] A. Konrad, U. Herr, R. Tidecks, F. Kummer, and K. Samwer, "Luminescence of bulk and nanocrystalline cubic yttria," *Journal of Applied Physics*, vol. 90, no. 7, pp. 3516–3523, 2001.

[16] D. Dosev, B. Guo, and I. M. Kennedy, "Photoluminescence of Eu^{3+}: Y_2O_3 as an indication of crystal structure and particle size in nanoparticles synthesized by flame spray pyrolysis," *Journal of Aerosol Science*, vol. 37, no. 3, pp. 402–412, 2006.

[17] M. A. Macêdo and J. M. Sasaki, "Processo de fabricação de pós nanoparticulados," Patent Pending 0203876-5/BR.

[18] H. Eilers, "Synthesis and characterization of nanophase yttria co-doped with erbium and ytterbium," *Materials Letters*, vol. 60, no. 2, pp. 214–217, 2006.

[19] F. A. Andrade de Jesus, R. S. Silva, A. C. Hernandes, and Z. S. Macedo, "Effect of pH on the production of dispersed $Bi_4Ge_3O_{12}$ nanoparticles by combustion synthesis," *Journal of the European Ceramic Society*, vol. 29, no. 1, pp. 125–130, 2009.

[20] C. T. Meneses, W. H. Flores, F. Garcia, and J. M. Sasaki, "A simple route to the synthesis of high-quality NiO nanoparticles," *Journal of Nanoparticle Research*, vol. 9, no. 3, pp. 501–505, 2007.

[21] W. Luan and L. Gao, "Influence of pH value on properties of nanocrystalline $BaTiO_3$ powder," *Ceramics International*, vol. 27, no. 6, pp. 645–648, 2001.

[22] P. J. R. Montes, M. E. G. Valerio, M. A. Macêdo, F. Cunha, and J. M. Sasaki, "Yttria thin films doped with rare earth for applications in radiation detectors and thermoluminescent dosimeters," *Microelectronics Journal*, vol. 34, no. 5–8, pp. 557–559, 2003.

[23] B. D. Cullity and S. R. Stock, *Elements of X-ray Diffraction*, Prentice Hall, Upper Saddle River, NJ, USA, 3rd edition, 2001.

[24] A. I. Rusanov, "Surface thermodynamics revisited," *Surface Science Reports*, vol. 58, no. 5-8, pp. 111–239, 2005.

[25] J. P. Jolivet, S. Cassaignon, C. Chanéac, D. Chiche, O. Durupthy, and D. Portehault, "Design of metal oxide nanoparticles: control of size, shape, crystalline structure and functionalization by aqueous chemistry," *Comptes Rendus Chimie*, vol. 13, no. 1-2, pp. 40–51, 2010.

[26] G. Cao, *Nanostrutures & Nanomaterials—Synthesis, Properties & Applications*, Imperial College Press, London, UK, 2004.

[27] G. Baldinozzi, J. F. Bérar, and G. Calvarin, "Rietveld refinement of two-phase Zr-doped Y_2O_3," *Materials Science Forum*, vol. 278-281, no. 2, pp. 680–685, 1998.

[28] Z. Fu, S. Zhou, T. Pan, and S. Zhang, "Preparation and luminescent properties of cubic Eu^{3+}:Y_2O_3 nanocrystals and comparison to bulk Eu^{3+}:Y_2O_3," *Journal of Luminescence*, vol. 124, no. 2, pp. 213–216, 2007.

[29] S. Setua, D. Menon, A. Asok, S. Nair, and M. Koyakutty, "Folate receptor targeted, rare-earth oxide nanocrystals for bi-modal fluorescence and magnetic imaging of cancer cells," *Biomaterials*, vol. 31, no. 4, pp. 714–729, 2010.

[30] J. W. Wang, Y. M. Chang, H. C. Chang et al., "Local structure dependence of the charge transfer band in nanocrystalline Y_2O_3:Eu^{3+}," *Chemical Physics Letters*, vol. 405, no. 4–6, pp. 314–317, 2005.

[31] S. J. Dhoble, I. M. Nagpure, J. G. Mahakhode, S. V. Godbole, M. K. Bhide, and S. V. Moharil, "Photoluminescence and XEL in Y_2O_3:Eu^{3+} phosphor," *Nuclear Instruments and Methods in Physics Research. Section B*, vol. 266, no. 15, pp. 3437–3442, 2008.